Investigating the Impacts of Oil Exposure and Changing Snow Cover on Sea Ice Diatom Communities in the Alaskan Arctic

Principal Investigator

Gwenn Hennon

College of Fisheries and Ocean Sciences, University of Alaska Fairbanks

Collaborator

Kyle Dilliplaine

College of Fisheries and Ocean Sciences, University of Alaska Fairbanks

December 2022

Final Reports

OCS Study BOEM 2022-062

BOEM Bureau of Ocean Energy Management

UAF University of Alaska Fairbanks

Contact Information:
uaf-cmi@alaska.edu
https://www.uaf.edu/cfos/research/cmi

This study was funded by the U.S. Department of the Interior, Bureau of Ocean Energy Management Alaska OCS Region and the University of Alaska Fairbanks under cooperative agreement M20AC10007. This report, BOEM 2022-062, is available through the Coastal Marine Institute and electronically from https://www.boem.gov/akpubs.

TABLE OF CONTENT

LIST OF FIGURES

LIST OF TABLES

ABSTRACT

Sea ice algae are a key component of the base of the Arctic food web, blooming early in spring to support zooplankton and other meiofauna when phytoplankton are not abundant. We isolated four strains of sea ice diatoms from sea ice cores collected near Utqiaġvik, Alaska, to examine the combined impacts of thinning sea ice/snow and crude oil exposure on these algae. The growth and maximum cell concentrations of four isolates (*Attheya septentrionalis, Fragilariopsis cylindrus, Synedropsis hyperborea* strains 1 and 2) were determined in a fully-factorial experiment with five irradiances (3–125 μmols photons m^{-2} s^{-1}) and twelve concentrations (0–8.7 mg L^{-1}) of Alaska North Slope (ANS) crude oil. These data were used to calculate ANS crude oil concentrations for 10% and 50% inhibition of growth (IC_{10} and IC_{50}). *F. cylindrus* was the most sensitive to ANS crude oil contamination with exponential growth IC_{10} of 1.4–5.3 mg L^{-1} and the only strain inhibited by 50% over the range of crude oil concentrations tested. There was evidence of interactions between irradiance and the impact of ANS crude oil exposure; *A. septentrionalis* had a significantly lower IC_{10} (higher sensitivity) under the highest irradiance while other strains had increasing IC_{10} (lower sensitivity) with increasing irradiance for some measures. These data were combined with *in situ* observations of sea ice thickness and irradiance to create a 1D model to assess how exposure to crude oil would impact sea ice algal biomass and diversity under different snow conditions. We found that algal diversity and biomass both decreased in a simulated ANS crude oil spill in the Alaskan Arctic, particularly under low snow conditions. Transcriptome experiments from sea ice diatom isolates and natural sea ice microbial communities were performed to assess the gene expression changes under oil contamination at different irradiances. Taken together, these data show that sea ice diatoms from the Alaskan Arctic have diverse responses to crude oil contamination, and responses can be modified by sea ice thickness and snow cover. Factors such as ice/snow conditions and sea ice algal community composition should be considered in determining the appropriate response to a crude oil spill in the Alaskan Arctic.

INTRODUCTION

Background

Oil and gas lease areas in the Beaufort Sea are adjacent to subsistence hunting and fishing areas that support the economies of many Arctic communities. In the Arctic, the base of the marine food web is supported by sea ice algae and phytoplankton. Diatoms are a prolific group of marine algae, contributing considerably to Arctic algal biomass in both ice and water (>95%; Szymanski and Gradinger 2016). The abundance and biomass concentrations of diatoms in sea ice, such as the ice-endemic *Nitzschia frigida* (Figure 1A), are ~1–3 orders of magnitude greater than in the underlying water column in early spring (Lee et al. 2008; Manes and Gradinger 2009), and these diatoms provide a significant pulse of high-quality food for pelagic and benthic fauna (Michel et al. 2006; Boetius et al. 2013). Studies estimate that ice algae contribute up to ~80% of carbon to various pelagic grazers over the Central Basin and ~70% to benthic infauna nearshore (Kohlbach et al. 2016, 2019); however, these estimates are highly uncertain. Algae and bacteria exist in close proximity within the confines of the sea ice brine channel system (Figure 1B) and likely have complex interactions ranging from competition for nutrients to mutualistic exchange of metabolites such as vitamins (Bowman 2015). Contamination of this marine environment might alter algal productivity, which could result in large-scale changes to the marine food web in the Arctic.

The dramatic loss of Arctic sea ice (Polyakov et al. 2017) is spurring the development of marine resources including shipping lanes, fisheries, and petroleum reserves (Arctic Council 2009; Eguíluz et al. 2016). Despite the expectation of ice-free summers by 2050 (Overland and Wang 2013; Wang et al. 2018), sea ice will continue to form during the Arctic winter and represent a hazard to the petroleum and maritime shipping industries. Potential effects of allowing oil and gas drilling in the Beaufort Sea include spills and gas blowouts that could contaminate the marine environment with crude oil, with spill response complicated by seasonally ice-covered waters. Mechanical and chemical oil spill response is limited to open water and, along with *in-situ* burning, they are imperfect cleanup strategies, leaving behind remnant oil that may contaminate sea ice that forms in the fall and, subsequently, impacting sea ice algal productivity in the spring.

The ability to respond to an oil spill is complicated by the presence of seasonal sea ice, regardless of spill source or size, and a worst-case oil spill in the Arctic may persist through winter until conditions are more favorable for a response the following summer (Blanken et al. 2017). In the fall of 2014, an unmanned fuel barge trapped in ice traveled 2,000 km through the Beaufort and Chukchi Seas with nearly 4,000 liters of diesel fuel on board (Ropeik 2015). The US Coast Guard could not free the trapped vessel due to limited icebreaking capacity. Models show that oil will accumulate and travel with ice movements $\geq$1000 km over a year (Blanken et al. 2017). Oil trapped in sea ice can remobilize under and within the ice through physical processes (e.g., ice deformation, melting, lead expansion/contraction) and spread with strong currents (AMAP 2007). Though stimulating to oil-degrading bacteria, microbes have limited access to oil encapsulated in ice, and it remains relatively unweathered, retaining many of its

volatile and toxic compounds (Boccadoro et al. 2018). Spills resulting from damaged vessels or blowouts, and redistribution of oil through dynamic ice processes, render the ice communities vulnerable to re-exposure at any time of the year, even if the point source has been contained.

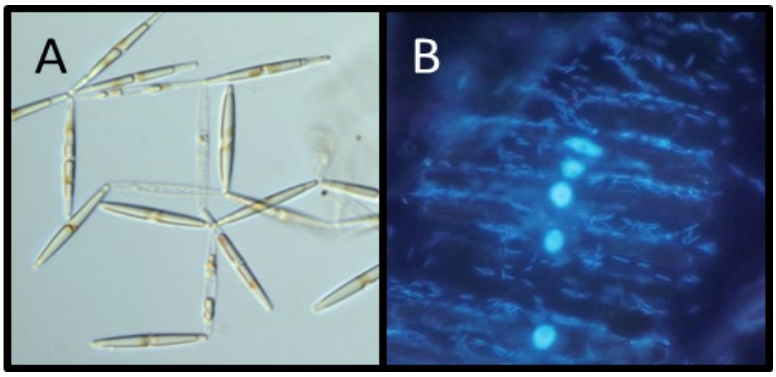

Figure 1. Sea ice diatoms and associated bacteria: (A) Light transmittance micrograph of the sea ice diatom *Nitzschia frigida* from Arctic pack ice and (B) DAPI stained epifluorescent micrograph of sea ice diatoms *Fragilariopsis* sp. and attached bacteria from landfast sea ice, Utqiaġvik, Alaska. (photo credit: Kyle Dilliplaine).

Crude oil and its distillates can inhibit growth in Arctic phytoplankton (Hsiao 1978; Aksmann and Tukaj 2008; Gilde and Pinckney 2012) and sea ice algae under high concentrations (Dilliplaine et al. 2021). While some organisms are sensitive to oil compounds, others are unaffected, even at relatively high concentrations (Gilde and Pinckney 2012; Ozhan et al. 2014). In addition, some diatom species are capable of biodegradation of crude oil distillates (Hong et al. 2008; El-Sheekh et al. 2013) and some ice-associated bacteria can degrade hydrocarbons as a source of energy (e.g., Colwellia; Garneau et al. 2016). Hennon et al. (2018) demonstrated that microbial interactions can be rapidly altered by anthropogenic stressors, however, the impacts of low-level hydrocarbon contamination on sea ice microbial communities remain unknown. A question remains whether sea ice algae communities have the genetic adaptations to resist oil toxicity or are sensitive to trace amounts of crude oil.

The mechanisms of oil toxicity include (1) accumulation of lipophilic oil compounds in the cell membrane that can cause membrane permeability and cell lysis (Sikkema et al. 1995), and (2) release of water-soluble compounds from crude oil that may stimulate the generation of reactive oxygen species (ROS) (Ozhan et al. 2015). High concentrations of ROS can react with important macromolecules (e.g., DNA, proteins, and lipids; Gutteridge 1995; Beckman and Ames 1997; Berlett and Stadtman 1997) causing oxidative stress and cell death. Fluorescent cell stains can be used to quantify membrane integrity and intracellular ROS. For example, Dilliplaine et al. (2021) observed a disruption of plastid DNA and the shape of the nucleus in sea ice algae from Utqiaġvik exposed to crude oil using the fluorescent DNA stain DAPI. Other stains are available to test membrane integrity including Sytox, a DNA stain that can only enter the cell when the membrane is compromised, indicating that a cell is no longer viable. Another fluorescent cell stain (CellROX) can travel through intact membranes and react with intracellular ROS and can be used to quantify oxidative stress in living or preserved cells. Oxidative stress

can cause cell death or decreased growth rates in both algae and bacteria, but it can also be combated by cell enzymes that safely destroy ROS compounds. ROS can also be generated as a byproduct of photosynthesis or respiration, and as a signaling molecule between microbes.

It has also been documented that ice algae are sensitive to rapid snow removal, with significant decreases in primary production due to photoinhibition at light levels above 50 uE (Juhl and Krembs 2010). High irradiance from reduced snow cover or thinning ice can cause oxidative damage to photosystem components of diatoms resulting in photoinhibition. As a safety valve, diatoms can shunt extra energy to photorespiration and release more dissolved organic carbon (Parker and Armbrust 2005). Differentiation of cell damage caused by oil contamination versus other sources of oxidative stress, such as high light, is impossible with physiological or stain assays. However, gene expression can reveal differences in metabolic pathways that are characteristic of photodamage versus chemical oxidative stress.

Genes involved in the oxidative stress response are well-characterized in diatoms and bacteria and include superoxide dismutase, catalase, and glutathione S-transferase. These genes are involved in the destruction of ROS through metabolic pathways and in intracellular signaling that may alter the expression of other core metabolic pathways such as photosynthesis and respiration. Photorespiration genes and pathways are also well-characterized in diatoms (Hennon et al. 2015) and have been activated in high-light conditions (Parker and Armbrust 2005). Genes involved with the metabolic breakdown of crude-oil components, such as polyaromatic hydrocarbons (PAH), have been well-characterized for bacteria and fungi and, to a much lesser extent, microalgae (Ghosal et al. 2016). It is unknown whether sea ice diatoms have these genes or express them under exposure to crude oil. The expression of PAH metabolism genes in sea ice bacteria and sea ice diatoms might indicate an ability to resist chemical damage or participate in bioremediation. Understanding how sea ice algae and bacteria regulate metabolic pathways when exposed to sublethal crude oil concentrations will provide critical insight into the mechanistic functions of Arctic sea ice microbial communities and provide genomic biomarkers for assessing their *in-situ* response to trace amounts of crude oil.

To investigate how an oil spill may alter primary production in the changing Arctic, we studied changes in ice microbe physiology and gene expression when exposed to sublethal concentrations of Alaska North Slope (ANS) crude oil and changes in snow cover. We are in the process of developing new genetic markers for sea ice algae, using *Fragilariopsis cylindrus* as a model species, to isolate the signals of physiological stress associated with crude oil contamination. These molecular tools could be used to uncover the change in natural sea ice communities exposed to low-level crude oil contamination, with broader implications for how these communities respond to changing snow conditions in the Arctic.

Hypotheses

1. Under elevated ANS crude oil contamination:
    a. Algal productivity will decrease; mortality and sublethal oxidative stress will increase.
    b. Sea ice algal genes associated with oxidative stress and bacterial genes associated with hydrocarbon degradation will be more highly expressed.

2. Under elevated irradiance/reduced snow cover:
   a. Algal productivity will increase at moderate light, then decrease at high light and sublethal oxidative stress will increase.
   b. Sea ice algal genes associated with oxidative stress, photoinhibition, and photorespiration will be more highly expressed.
3. With significant interaction between elevated irradiance/reduced snow cover and ANS crude oil contamination:
   a. Sea ice algal production will be further depressed by the combination of crude oil contamination and high light compared with either stressor independently.

Objectives

1. Determine the impact of varying crude oil concentrations and irradiance on the productivity, mortality, and sublethal oxidative stress of:
   a. sea ice diatom *Nitzschia frigida.**
   b. a natural sea ice algal and bacterial community.
2. *De novo* transcriptome assembly of *N. frigida*** expressed genes.
3. Identify genes indicative of ANS crude oil exposure and decreased snow cover with the use of (meta)transcriptomics in bottle incubations with:
   a. sea ice diatom *Nitzschia frigida.***
   b. a natural sea ice algal and bacterial community.

* We could not use *Nitzschia frigida* so alternate algae were used, see Methods.

**We could not use *Nitzschia frigida* so we completed transcriptomics on *Fragilariopsis cylindrus* and *Synedropsis hyperborea*, two sea ice diatoms with contrasting crude oil sensitivities. A genome assembly is already available for *Fragilariopsis cylindrus*, thus a transcriptome assembly was not necessary for the transcriptome analysis.

METHODS

Selection of Sea Ice Algal Strains

We proposed to test the responses to light and ANS crude oil contamination of an isolate of the sea ice diatom *Nitzschia frigida*. However, the culture was lost in the spring of 2020, when our collaborator faced restricted laboratory access due to COVID-19 and was unable to maintain the culture. Instead, we established new uni-algal cultures of algae isolated from sea ice cores collected in Utqiaġvik in May 2020. This allowed us to study a broader range of algal strains native to the region of interest, with the added benefit that the freshly isolated cultures had less time to be altered by cultivation. We characterized the crude oil sensitivity of four sea ice diatoms (*Attheya septentrionalis, Fragilariopsis cylindrus, Synedropsis hyperborea* str. 1 and 2) instead of the one diatom (*Nitzschia frigida*) that we originally proposed to study. This allowed us to extrapolate how a mock community composed of four diatoms would be impacted by a hypothetical oil spill before the spring bloom, and we explored this with a simple 1D model forced by *in situ* irradiances relevant to the Alaskan Arctic.

Sea Ice Coring and Sample Collection

Cores for sea ice algal cultivation and batch culture experiments were collected from landfast sea ice offshore of Utqiaġvik, Alaska (Figure 2) on May 25, 2020, and April 25–26, 2022. For sea ice algal cultivation, the bottom ~10 cm of core was slowly melted in the dark with the addition of filtered seawater to minimize osmotic shock (Garrison and Buck 1986). Aliquots of the core melt material were diluted into f/25 +Si medium according to (Guillard and Ryther 1962) using natural seawater (S=36) collected from the Gulf of Alaska at a depth exceeding 500 m. In brief, seawater was sterile-filtered with a 0.2 µm sterivex filter, macronutrients and trace metals were added, and the media was autoclaved. To complete media preparation, sterile-filtered (0.2 µm) vitamins were added after cooling to avoid denaturation of the vitamins.

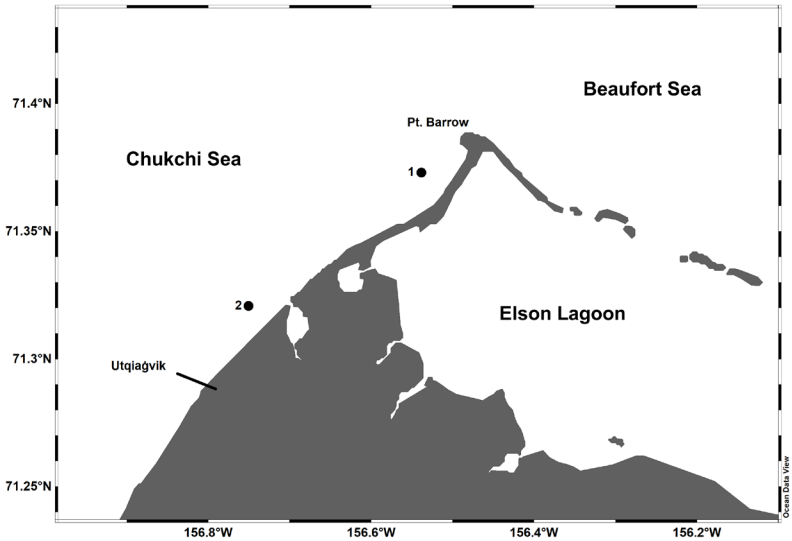

Figure 2. Study area near Utqiaġvik, Alaska. Location of sea ice core sampling for algal cultivation (1) and natural community batch experiments (2).

For batch culture experiments with natural communities, biota was collected from sea ice near Utqiaġvik, Alaska (Chukchi Sea; 71° 19' 15.1" N, 156° 45' 2.74" W, Figure 2) on April 25, 2022. A small flat pan of ice, approximately 100 m^2, was selected to provide a uniform sampling location. Triplicate samples were collected using a 9-cm inner diameter Kovak's corer for DNA, meiofauna enumeration, and chlorophyll *a*. The bottom 10 cm was sectioned at the intervals of 0–2, 2–5, and 5–10 cm where 0 represents the ice-water interface. Incident and under-ice irradiance were measured continuously and simultaneously adjacent to the sampling area using an LI-COR LI-1500 data logger with planar and spherical quantum sensors. Snow was cleared from the ice at the end of the sampling day to establish under-ice irradiance under snow-free ice. Single cores were collected for temperature and salinity; the temperature was measured every 10 cm and salinity samples were sectioned every 5 cm. At the laboratory, biological sections were melted with the addition of filtered seawater to avoid osmotic stress (Garrison and Buck 1986) and immediately filtered after homogenization by gentle inversion of the sample for 60 seconds. Salinity samples were melted in a sealed plastic jar at room temperature and measured using a

YSI conductivity probe. Bulk biota was collected from the same location on April 26, 2022. The bottom 2 cm of ice from 12 cores of 20 cm diameter were melted with the addition of seawater pumped through a 20 µm prefilter from under the ice. Ice was melted at 4°C at an *in situ* irradiance of 15 µmols photons m^{-2} s^{-1} and transferred to 0°C when all ice was melted. Half of the biota was concentrated on a 4 µm mesh sieve before transport to Fairbanks, Alaska.

Isolation and Identification of Sea Ice Algal Strains

Mixed sea ice algal cultures were maintained at approximately 15 µmols photons m^{-2} s^{-1} in 25 mm culture tubes at 4°C with a 12-hour light-dark cycle using a low-temperature incubator for propagation and isolation. Sea ice algae were isolated from these mixed cultures using 1.25% agar plates containing f/25 +Si medium following Kimura and Tomaru (2013). Briefly, 5 ml of diluted cultures were added to the agar plates allowing cells to settle for 12 hours before decantation. Plates were left to incubate for approximately one month until colonies were visible. Single colonies were selected using an inoculation loop, resuspended in f/25 +Si medium, and maintained by transfer to fresh medium every 2 to 4 weeks. Isolates were confirmed to be unialgal by light microscopy. Identification to species level was performed using a combination of light microscopy, scanning electron microscopy (FEI Quanta 200), and 18S rRNA gene sequencing (Table 1).

Table 1. Sea ice diatom isolate characteristics and identification methods. Isolate genus and species identification, morphotypes, geometric shapes used to calculate biovolume (µm^3), and carbon content (pg cell ^{1}). Identification methods included light microscopy (LM), 18S rRNA gene sequencing (DNA), and scanning electron microscopy (SEM).

Isolate	Morpho-type	Geometric Shape	Biovolume (µm^3)	Carbon (pg cell^{-1})	Identification Method
Attheya septentrionalis	centric	cylinder	186	122	LM, DNA
Fragilariopsis cylindrus	pennate	rectangular prism	142	104	SEM, LM, DNA
Synedropsis hyperborea str. 1	pennate	irregular	117	93	SEM
Synedropsis hyperborea str. 2	pennate	irregular	80	75	SEM

Crude Oil WAF Preparation and Chemical Analyses

ANS crude oil was used as a regionally representative oil for this experiment. ANS crude was provided by Alyeska Pipeline Services from Pump Station 1 at the Trans-Alaska Pipeline entry point. The water-accommodated fraction (WAF) of crude oil was prepared according to the Chemical Response to Oil Spills: Ecological Research Forum (CROSERF; Aurand and Coelho 2005) and Singer et al. (2000). Briefly, 10.5 L f/25 + Si medium was added to a 20-L acid-cleaned glass aspirator bottle and 12 g L^{-1} of ANS crude oil was gently added to the surface of the water. The mixture was stirred continuously for 48 hours on a stir plate to produce a vortex of approximately 25% of the medium height without the formation of droplets at -1°C in the dark. WAF was collected from below the oil layer through the spigot and was free of any visible

oil. WAF dilutions were immediately prepared for the dose-response experiments, ranging from 9.1–100%, by mixing with clean f/25 + Si medium in sterile, acid-cleaned, glass containers and finally diluted by 10% from the addition of cell culture volume.

Samples for chemical analysis were collected in 200 ml acid-cleaned amber glass jars with Teflon lined lids and stored at -20°C until further processing, approximately 12 months from collection. Chemical analyses of the stock WAF (100%) were conducted at Emax Laboratories, Inc. (Torrance, CA) using the Alaska Department of Environmental Conservation methods for n-alkanes in the diesel range organics (DRO; C_{10}-C_{25}); gas chromatography equipped with a flame ionization detector (GC-FID; Agilent G1530N; Figure 1) was used for residual range organics (RRO; C_{25}-C_{36}) and total petroleum hydrocarbons (TPH; C_8-C_{40}) according to methods AK 102/103 (ADEC 2002a; b). Petroleum concentrations in the dilutions were calculated from the stock concentration as it is conserved linearly (Mcfarlin et al. 2011; Gardiner et al. 2013).

Experimental Design

Experiments were conducted in a cold room located at the University of Alaska Fairbanks. Sea ice algal isolates were transferred to optically clear, untreated, 96-well flat-bottom plates and incubated at -1°C to approximate the temperature of the skeletal layer of sea ice. Plates were set on rigid icepacks (40 x 40 x 1 cm) with a melting point of -1°C to maintain a stable temperature. Five light conditions (3, 10, 20, 50, and 125 µmols photons m^{-2} s^{-1}) were established using LED lights with a 12-hour light-dark cycle. Photosynthetically active radiation (PAR) was measured with a Li-190R planar light sensor (LI-COR; Lincoln, NE) and intensity was tuned using a combination of voltage regulators and neutral density screens. Cultures were transferred to fresh medium once late exponential growth was achieved (every 1–2 weeks) and allowed to acclimate to light conditions over 70 days, ensuring cultures were photoacclimated before the determination of growth physiology.

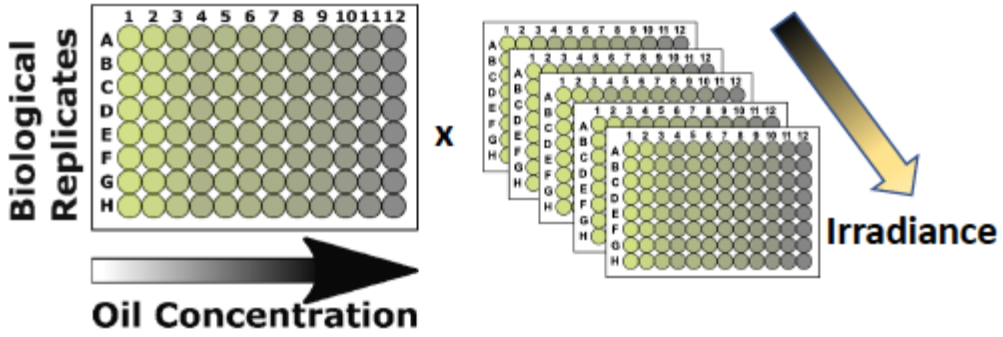

Figure 3. Layout of plate experiment design with oil and light gradients. Sea ice diatoms on 96-well plates under a range of concentrations of crude oil-water accommodated fraction and grown under a gradient of light to determine the IC10 and IC50 under five light conditions.

Two sets of 96-well plates (experimental and unoiled) were prepared for each of the four isolates and five light conditions used in the experiment, 40 plates total (Figure 3). Experimental

plates contained a linear dilution gradient of ANS WAF, from 0–90% working concentration, for a total of 12 treatments, each with 8 replicates per plate (Figure 3). Unoiled plates were used exclusively for cell harvest during the experiment and contained an oil-free medium (0% WAF). Photoacclimated cultures were transferred to each well, after pipetting to mix, at a 1:9 volume ratio of cell culture to WAF. Median initial cell densities within wells ranged from 9.5–11.5 x 10^3 cells mL^{-1}. Fluorescence was measured daily using a SpectraMax Gemini EM plate reader (Molecular Devices, San Jose, CA) at wavelengths for *in vivo* chlorophyll *a* fluorescence (460 ex 665 em) 8 hours after lights were turned off. Experiments were ended after leveling off, or decline, in fluorescence was observed. Some taxa did not completely level off by the end of the experiment (32 days).

Dose-response Crude Oil and Irradiance Experiments

Cells were harvested from the unoiled plates four times during the experiment; four replicate samples were collected from each plate and preserved with a 2% final concentration of Lugol's solution and stored at 4°C until further processing (< 6 months). Each fixed sample was a pool of four adjacent wells, and relative fluorescence was averaged among these four wells for the calculation of cell concentration. Cells were counted using a Sedgewick rafter counting chamber (Forestry Suppliers Inc., Jackson, MS) and at least 100 cells, or 10 µl total volume, were counted for each sample. *F. cylindrus* and *A. septentrionalis* were manually counted using an inverted Nikon Eclipse TE2000-U at 400x. *S. hyperborea* cells were counted from micrographs taken with a Teledyne Photometrics Prime BSI camera with automated image analysis using the Cell Counter plugin (v. 3.0.0) for imageJ (Schneider et al. 2012). Image analysis counts were found to closely match manual counts with an underestimation of < 5%. The relationships between relative chlorophyll *a* fluorescence and cell concentration were determined using linear regression with an intercept forced through 0 for each combination of isolate and irradiance (Figure 3). Relative fluorescence measured in the experimental plates was converted to cell concentration by multiplying the blank-corrected value by the empirically-determined slope. Exponential growth rates (µ, d^{-1}) were calculated as the log-linear change in cell concentration using the 'all_easylinear' function described by Hall et al. (2014) for each well. Maximum cell concentration was calculated as the maximum observed cell concentration during the experiment. The error was determined as the sum of squares using calculated errors associated with cell counts and biological replication.

Physiological Data Analysis

Growth rate versus irradiance curves were generated for photoacclimated cultures of each of the four isolates using the unoiled control wells (Figure 2). The R package 'phytotools' (Silsbe and Malkin 2015) was used to fit four models and estimate growth parameters (Table 1) according to Eilers and Peeters (1988), Jassby and Platt (1976), Platt et al. (1980), and Webb et al. (1974). The best model was selected by minimizing the squared sum of the residuals (SSR; Burnham and Anderson 2004) and Akaike's information criterion (AIC), which balances the goodness of fit with the complexity of the model (Spiess and Neumeyer 2010).

Dose-response curves were generated using species-specific maximum growth rates and concentrations using nonlinear models fit with the R package 'drc' (Knezevic et al. 2007). Models with and without irradiance as a factor were tested for significance using ANOVA ($p < 0.05$), irradiance was significant and included as a factor in all models. Three curves (*A. septentrionalis* irradiance level 50, *S. hyperborea str.* 1 irradiance level 10, *S. hyperborea str.* 2 irradiance level 20) were removed before model fitting due to the presence of a positive trend resulting in model direction reversal and fit instead using linear regression. The best-fitting model was selected using AIC, and visual inspection when values were close (AIC < 10). Models for growth rate have a fixed lower limit of 0 with the assumption that there will be no growth at some concentration of WAF (not observed). The lower limit for dose-response curves generated using the maximum concentration was set to the median initial concentration per species. The concentrations required to inhibit growth rate or maximum concentration by 10% (IC_{10}) and 50% (IC_{50}) were calculated from the model fits (Knezevic et al. 2007). Due to the lower limit set point variability in models used between growth rate and cell concentration, IC values are absolute for growth rate and relative to initial cell concentrations for maximum concentration.

Modeling the Impact of Oil Exposure and Snow Cover on Algal Growth and Diversity

A 1D model was used to simulate the growth of a simplified ice algal community over a spring-bloom period in the presence and absence of crude-oil exposure with realistic under-ice irradiance. The under-ice irradiance (UI_{PAR}) was calculated using the Beer-Lambert law (Equation 1) and forced with observations of incident irradiance and sea-ice thickness in the Alaskan Arctic. Incident irradiance (PAR; 30-minute average) was downloaded from the National Ecological Observatory Network (NEON) at the Utqiaġvik, Alaska station (BARR) for the years 2020 and 2022. PAR data was distilled to a single daily irradiance value (I) by averaging the irradiance within a 12-hour window centered on solar noon from March 1 to May 15 (Figure S4.C). A daily sea ice thickness (Hi) value was calculated as the average of all daily point measurements (every 15 minutes) measured at a Sea Ice Mass Balance station in 2014 (Chukchi Sea; 71°22' N, 156°31' W) using an upward-facing acoustic transducer ((NSF Arctic Data Center 2009); Figure 4E). Fixed snow depths (Hs) were chosen to simulate under-ice light intensities under snow depths ranging from 0 to 20 cm (Figure 4D). The integrated PAR attenuation coefficients for snow (*K*s, 11) and ice (*K*i, 3.6) were derived from McDonald et al. (2015), *K*i was adjusted to 2.6, within the reported confidence interval, to include upwelling irradiance as measured *in situ* (May 2022) using a spherical quantum sensor (LI-COR).

$$UI_{PAR} = Ie^{(-KiHi)+(-KsHs)} \quad \text{Equation 1}$$

The simulated ice algal community was composed of the four isolates investigated in this study seeded at equal starting concentrations. Cell abundance (A_d) was calculated for each day assuming exponential growth (Equation 2) of cell abundance from the previous time step (A_{d-1}). Isolate-specific growth rates (μ) were a function of irradiance (UI_{PAR}) and one of two oil

concentrations determined empirically in this study: no oil contamination, and at the highest tested concentration (8.7 mg L^{-1} TPH). A loss term (g) was fixed at 0.06 d^{-1}. Cell abundance (A) at the initial time step was set at 1000 cells for each of the four algae. Cell concentrations were converted to carbon content (C, pg C) using the isolate-specific biovolume (BV, μm^3) and the relationship derived from all data during exponential growth from Lomas et al. (2019).

$$A_d = A_{d-1} e^{(\mu - g)} \qquad \text{Equation 2}$$

Transcriptome Batch Culture Experiments

Isolates: The sea ice algal isolates, *F. cylindrus* and *S. hyperborea str.* 1 were incubated in optically clear 2-L polycarbonate bottles with continuous light for five days. Irradiances of 3, 20, and 125 µmols photons m^{-2} s^{-1} were chosen to simulate irradiance under high snow cover, low snow cover, and open water. Fresh WAF batches were prepared at the start of each of the two isolate transcriptome experiments. f/12.5 + Si medium was used instead of the f/25 used in the plate experiments, to avoid any potential nutrient limitation while growing larger cultures. Bottles were prepared in triplicate for each oil and light condition. Each bottle contained 1,550 ml of diluted WAF and 200 ml of light-acclimated algal culture (total volume = 1,750 ml), with final WAF dilutions of 0, 42, and 82%. *In vivo* chlorophyll and photosynthetic efficiency (Fv/Fm) were measured daily using a handheld *Aqua*Flash fluorometer (Turner Designs, San Jose, CA). Aliquots of each bottle (250–450 ml) were filtered ($\leq$ 30 minutes when possible) for RNA using 5-µm polycarbonate membrane filters during mid-exponential growth (i.e., days 3 or 5). All surfaces, tools, and gloves were cleaned using 70% ethanol and RNaseZap (Invitrogen, Waltham, MA). Filters were folded, deposited into cryovials, immediately frozen in liquid nitrogen, and stored at -80°C until extraction. All oil analyses were conducted at Emax Laboratories, Inc. (Torrance, CA) using gas chromatography equipped with a flame ionization detector (GC-FID; Agilent G1530N) following methods AK 102/103 (ADEC 2002a; ADEC 2002b) for n-alkanes in the Diesel Range Organics (DRO; C_{10}-C_{25}), Residual Range Organics (RRO; C_{25}-C_{36}), and Total Petroleum Hydrocarbons (TPH; C_8-C_{40})

Natural Community: An experiment was conducted using a natural sea ice microbial community with the following modifications: irradiances (15, 40, and 125 µmols photons m^{-2} s^{-1}) were chosen to represent snow-covered ice, snow-free ice, and open water conditions. f/2 + Si medium was used to further alleviate concerns of potential nutrient limitation. The natural community was incubated at a stable 15 µmols photons m^{-2} s^{-1} until the start of the experiment, <72 hours after collection, and was not light acclimated to other irradiances. Two WAF treatments were used, 0 and 42% WAF final concentration. 10–35 ml aliquots were sampled daily from each bottle for chlorophyll *a* and DNA using 25mm GF/F and 0.2 µm polycarbonate membrane filters. All filtration for RNA occurred on day 5; a final chlorophyll *a* and DNA filtration was conducted on day 9. DRO, RRO, TPH, and PAHs and Gas Range Organics (GRO; C_6-C_{10}) were determined according to methods AK 102/103 (ADEC 2002a; ADEC 2002b).

DNA and RNA Extraction and Sequencing

DNA was extracted from the field samples using the NucleoMag DNA/RNA Water kit (Macherey Nagel, Düren, GE) using 5-ml bead tubes. Extraction was conducted according to the manual for filters sized 47 mm. 25 mm DNA filters collected from the bottle experiments were extracted using the MagMax Microbiome Ultra Nucleic Acid extraction kit (ThermoFisher Scientific, Waltham, MA). The V4 regions of the 16S and 18S rRNA genes were amplified for each sample. 16S rRNA gene amplicons were produced using the revised Earth Microbiome Project primers (515FB and 806RB; Caporaso et al. 2012; Apprill et al. 2015; Parada et al. 2016). 18S rRNA gene amplicons were generated using the primers TAReuk454FWD1 and TAReukREV3 (Stoeck et al. 2010). Primers were modified with TaggiMatrix indices to enable the pooling of samples before adaptation with Illumina sequencing adapters (Glenn et al. 2019). Samples were sequenced on an Illumina MiSeq at the University of Alaska Anchorage.

RNA was extracted from filters using the RNeasy PowerPlant kit (Hilden, GE). Filters were transferred to bead tubes containing extraction buffer immediately after thawing on ice. Filters were beaten using a Retsch MM300 TissueLyser lab vibration mill mixer for 45 seconds at 30 Hz. Extraction proceeded according to the manual with the addition of RNase-free DNase (Qiagen). RNA integrity was checked using an Agilent Bioanalyzer RNA 6000 chip (Agilent, Santa Clara, CA) before sending to Novogene Corp (Sacramento, CA) for library preparation and sequencing on an Illumina platform. Each sample received at least 115 million reads.

RESULTS

Characterization of Sea Ice Diatom Isolates

To assess the potential for interacting anthropogenic impacts on the Alaskan Arctic ecosystem, sea ice algae were isolated near Utqiaġvik, Alaska. Four diatoms, *Attheya septentrionalis, Fragilariopsis cylindrus,* and two strains of *Synedropsis hyperborea* were selected from among these isolates based on their prevalence in the original samples and pan-Arctic distribution (Hasle et al. 1994; Poulin et al. 2011). The four diatom isolates were diverse in morphology (Figure 4) and varied in biovolume, with the largest being *A. septentrionalis*, followed by *F. cylindrus*, and *S. hyperborea* (Table 1). The two strains of *S. hyperborea* varied in morphology and size with *S. hyperborea str. 1* being longer and thinner compared to the shorter and broader *S. hyperborea str. 2* (Figures 4 C, D).

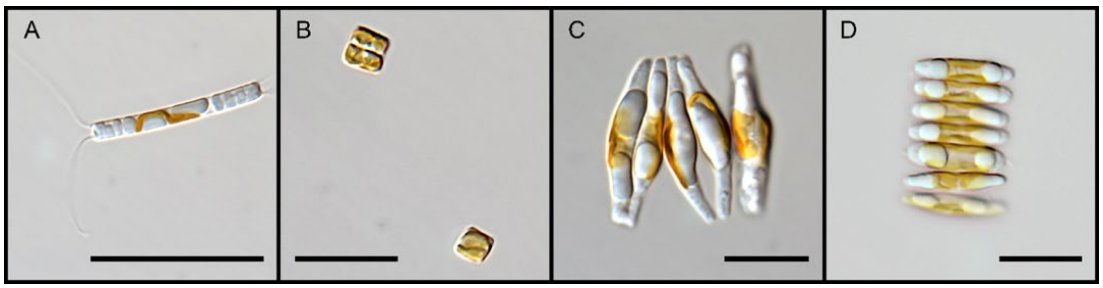

Figure 4. Sea ice diatoms isolated near Utqiaġvik, Alaska. Differential interference contrast micrographs of (A) *Attheya septentrionalis*, (B) *Fragilariopsis cylindrus*, (C) *Synedropsis hyperborea* strain 1, (D) *Synedropsis hyperborea* strain 2. Scales bars are 20 µm.

The sea ice diatom isolates also varied in light-acclimated growth rates (Figure 5). *A. septentrionalis* and *F. cylindrus* did not exhibit photoinhibition within the range of tested irradiances (Figures 5A, B). The growth-irradiance model that best fit the data did not parameterize photoinhibition (Table 2; Webb et al. 1974). *F. cylindrus* had the highest and lowest growth rates across the irradiances tested (Figure 5B). A growth-irradiance model with photoinhibition (Eilers and Peeters 1988) was selected as the best fit for the two strains of *S. hyperborea* (Table 2, Figures 5C, D).

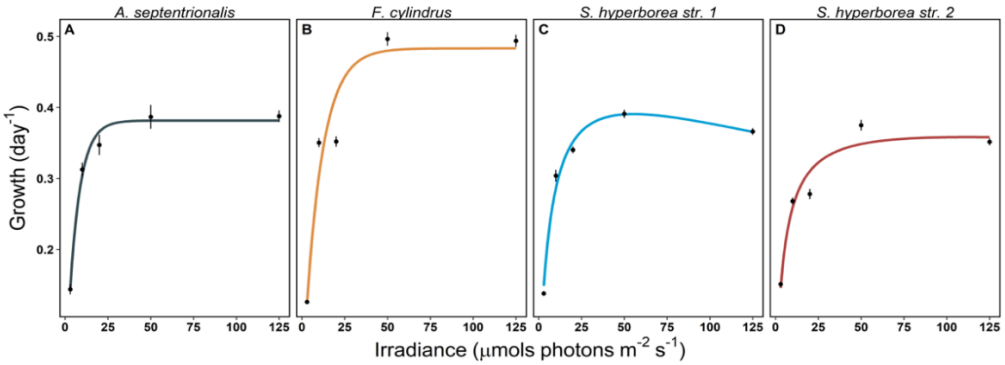

Figure 5. Growth-irradiance curves for sea ice diatom isolates. Exponential growth (day^{-1}) versus irradiance (µmols photons m^{-2} s^{-1}) for four strains of sea ice diatoms; (A) *Attheya septentrionalis*, (B) *Fragilariopsis cylindrus*, (C) *Synedropsis hyperborea* str. 1, and (D) *Synedropsis hyperborea* str. 2. Points indicate the light-acclimated growth rates of each strain (mean ± SE; n=8), and lines indicate growth-irradiance model fits (model type and parameters in Table 1).

Table 2. Growth-irradiance model type and parameter estimates for sea ice diatom isolates. Model type; Webb et al. 1974 or Eilers and Peeters 1988, and parameters for model fitting: initial slope of the growth irradiance curve (α; growth (d^{-1}) (µmols photons m^{-2} s^{-1})$^{-1}$), irradiance at the onset of saturation (e_k; µmols photons m^{-2} s^{-1}), and the irradiance at the onset of photoinhibition (e_{phot}; µmols photons m^{-2} s^{-1}) ± standard error (SE). nd is not determined.

		Model Parameter Estimates		
Isolate	**Model**	**α ± SE**	**e_k ± SE**	**e_{phot} ± SE**
Fragilariopsis cylindrus	Webb	4.8 ± 0.3 x 10^{-2}	10.1 ± 0.7	nd
Attheya septentrionalis	Webb	6.1 ± 0.2 x 10^{-2}	6.3 ± 0.2	nd
Synedropsis hyperborea str.1	Eilers-Peeters	7.2 ± 0.3 x 10^{-2}	5.5 ± 0.1	55.4 ± 2.4
Synedropsis hyperborea str.2	Eilers-Peeters	7.8 ± 0.7 x 10^{-2}	4.6 ± 4.7	111.8 ± 52.5

The irradiance at the onset of inhibition, e_{phot}, was indistinguishable (high standard error) between the two strains of *S. hyperborea* (Table 2). Other growth-irradiance model parameters differed by strain (Table 2). The initial slope of the curve (α) was the smallest for *F. cylindrus* followed in increasing order by *A. septentrionalis* and then both strains of *S. hyperborea,* which did not differ significantly. The saturating irradiance, e_k, followed the inverse pattern with *F. cylindrus* highest followed in decreasing order by *A. septentrionalis* and both strains of *S. hyperborea,* which did not differ significantly. (Table 2).

Sublethal Impacts of Crude Oil Modified by Irradiance

To test the impact of oil exposure on diatom growth physiology, isolates were transferred to oil-contaminated media generated using ANS crude oil at environmentally relevant temperatures (-1 °C). Concentrations of petroleum hydrocarbons were measured from the undiluted water accommodated fraction (WAF) at the onset of the experiment as technical replicates (n=3). Concentration (mean ± SD; n=3) of TPHs (C_8-C_{40}) was 9.7 ± 0.6 mg L^{-1}; DRO (C_{10}-C_{25}) was 3.0 ± 0.0 mg L^{-1}; and RRO (C_{25}-C_{36}) was 0.6 ± 0.3 mg L^{-1}. Approximately 60% of the TPHs were not attributed to the DRO or RRO fractions. TPH also includes hydrocarbons in $C_{8\text{-}9}$ and $C_{38\text{-}40}$ size ranges, and nearly all the additional TPH concentration was contributed by the lower molecular weight $C_{8\text{-}9}$ fraction.

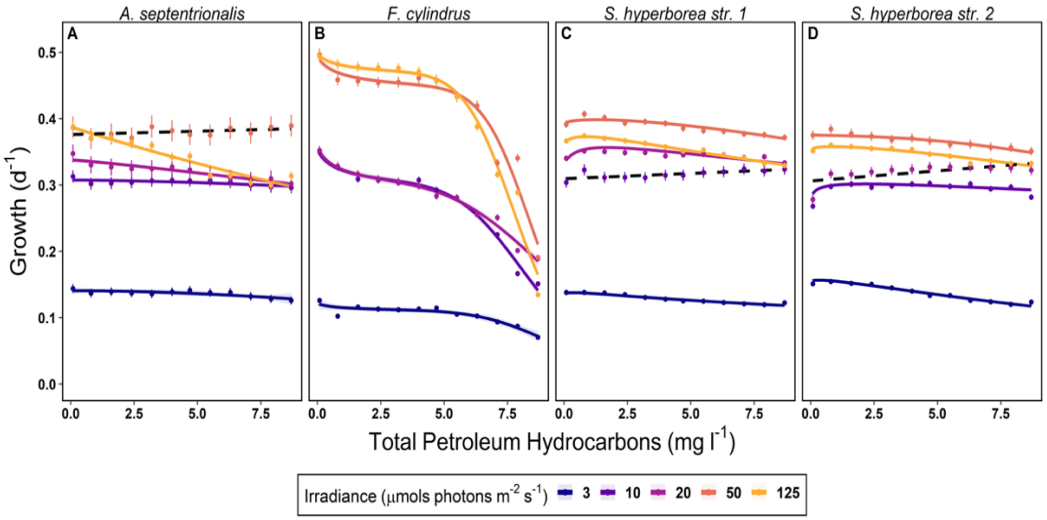

Figure 6. Dose-response curves of growth rate versus crude oil as modified by irradiance. Exponential growth rate (day^{-1}) in media contaminated with total petroleum hydrocarbon concentrations (mg L^{-1}) of four sea ice diatoms A) *Attheya septentrionalis*, B) *Fragilariopsis cylindrus*, C) *Synedropsis hyperborea* str. 1, D) *Synedropsis hyperborea* str. 2. Under irradiance of 3 (blue), 10 (purple), 20 (maroon), 50 (orange), 125 (yellow) µmols photons m^{-2} s^{-1}. Data points are the mean ± SE (n=8). The shaded ribbon is the 95% confidence interval of the model fit. Black dashed lines are linear fits; see Table 2 for model types.

Sea ice diatom isolates were evaluated based on their exponential growth rates in the presence of ANS crude oil using dose-response curves. There were inter- and intraspecific variability in sea ice algal growth rate responses to crude oil contamination that was modified by irradiance (Figure 6). *A. septentrionalis* had a generally low sensitivity except at the highest irradiance level where a relative decline in growth rate of ~19% was observed at the highest tested TPH concentration (Figure 6A). IC_{10} fell within the tested concentrations for *A. septentrionalis* at the lowest (3) and highest (125) irradiance levels, with a significantly lower IC_{10} at the highest irradiance level (Table 3). *F. cylindrus* was the most sensitive to crude oil contamination (Figure 6B), and the only isolate to exhibit inhibition of the growth rate by 50% (IC_{50}) within the tested concentrations (Table 3). IC_{10} for *F. cylindrus* were significantly

different ($p < 0.05$) between the intermediate (10, 20) and the high (50, 125) irradiance levels; all three IC_{50} concentrations, irradiance levels 10, 50 and 125, were significantly different from one another (Table 3). *S. hyperborea str. 1* was the least sensitive isolate when comparing calculable IC_{10} values, though both strains of *S. hyperborea* exhibited low sensitivity (Figures 6C, D; Table 3). Both strains of *S. hyperborea* exhibited a significant hormetic response for an intermediate light level (Figures 6C, D). IC_{10} fell within the range of tested concentrations only at the lowest irradiance level (3) for both strains of *S. hyperborea* and strain 2 exhibited a significantly lower threshold than strain 1 (Table 3). The three conditions fit with linear models, *A. septentrionalis* (irradiance 50), *S. hyperborea str. 1* (irradiance 10), and *S. hyperborea str. 2* (irradiance 20), exhibited an increase in growth rate with increasing TPH across the range of tested concentrations (Figures 6A, C, D).

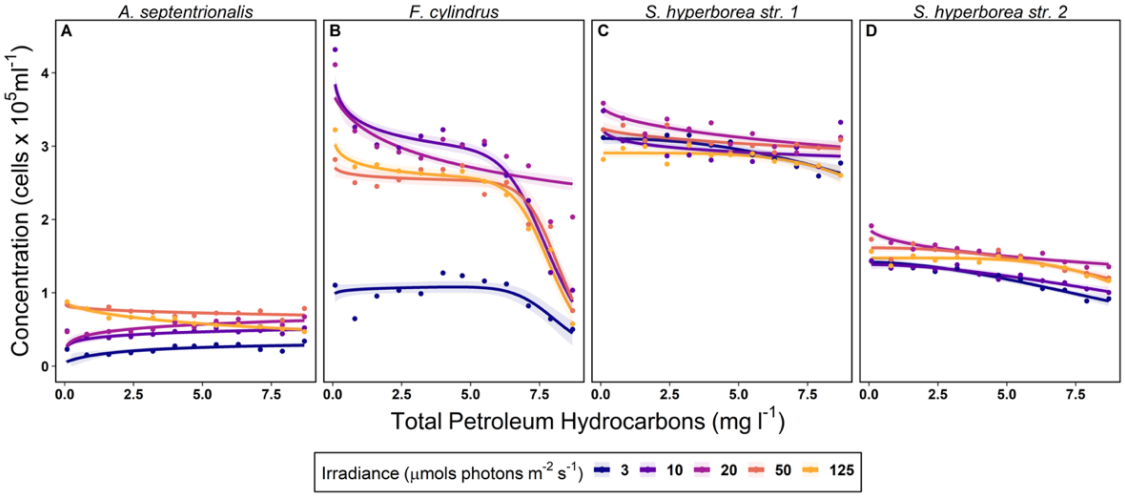

Figure 7. Dose-response curves of maximum cell concentration versus crude oil as modified by irradiance. Maximum cell concentration (cells x 10^5 mL^{-1}) in media contaminated with total petroleum hydrocarbon concentrations (mg L^{-1}) of four sea ice diatom isolates as in Figure 5. Modified by growth under irradiance of 3 (blue), 10 (purple), 20 (maroon), 50 (orange), and 125 (yellow) µmols photons m^{-2} s^{-1}. Data points are the mean $\pm$ SE (n=8). The shaded ribbon is the 95% confidence interval of the model fit.

As with exponential growth rate, there was inter- and intraspecific variability in the maximum cell concentration when exposed to crude oil that was modified by irradiance (Figure 7). The dose-response curves exhibited a greater decline in maximum cell concentrations as reflected by more calculable IC values relative to growth rate (Table 3). *A. septentrionalis* was the least sensitive to changes in maximum cell concentration (Figure 7A) with a general positive increase in concentration with increasing TPH at irradiances below 50 µmols photons m^{-2} s^{-1}, above which, the maximum concentration decreased. Decreases in maximum cell concentrations were reflected in the IC_{10} at irradiance levels 50 and 125 but were not significantly different from one another (Table 3). *F. cylindrus* was, again, the most sensitive isolate to TPH exposure (Figure 7B), and the only isolate inhibited by 50% (IC_{50}; Table 3). IC_{10} concentrations for *F. cylindrus* were significantly different between two groups of irradiance levels; 3 and 50 were

significantly higher ($p < 0.05$) than 10, 20, and 125, and the IC_{50} mirrored this grouping and significance, with the exclusion of irradiance 20, which fell outside the range of tested TPH concentrations (Table 3). Maximum concentrations varied between strains of *S. hyperborea,* with strain 2 growing to approximately half the concentration of strain 1. Although growth rates were relatively constant or even increasing with increasing TPH concentrations for S. hyperborea (Figures 6 C, D), maximum cell concentration declined at all irradiance levels for both strains (Figures 7 C, D). Nearly all irradiance levels had an IC_{10} that fell within the range of tested TPH concentrations for both strains of *S. hyperborea* reflecting the increased sensitivity of maximum cell concentration relative to the growth rate (Table 3).

Table 3. Inhibitory concentrations of total petroleum hydrocarbons by species and irradiance. Concentration of ANS crude oil total petroleum hydrocarbons (mg L^{-1}) mean ± SE that inhibited by 10% or 50% (IC_{10}, IC_{50}) exponential growth rate (μ) and maximum cell concentration (k) under irradiances ranging from 3–125 (μmols photons m^{-2} s^{-1}).

			Irradiance (μmols photons m^{-2} s^{-1})				
IC (%)	**Isolate**	**Measure**	**3**	**10**	**20**	**50**	**125**
10	*A. septentrionalis*	μ	> 8.7	> 8.7	8.2 ± 0.6	> 8.7	3.4 ± 0.3
10	*A. septentrionalis*	k	> 8.7	> 8.7	> 8.7	2.1 ± 2.2	0.5 ± 0.3
10	*F. cylindrus*	μ	5.0 ± 1.5	1.8 ± 0.5	1.4 ± 0.4	5.2 ± 0.4	5.3 ± 0.2
10	*F. cylindrus*	k	7.2 ± 0.5	0.1 ± 0.0	0.0 ± 0.0	5.7 ± 1.9	0.3 ± 0.1
10	*S. hyperborea str. 1*	μ	5.6 ± 0.0	> 8.7	> 8.7	> 8.7	> 8.7
10	*S. hyperborea str. 1*	k	6.9 ± 0.6	0.3 ± 0.3	2.5 ± 1.4	> 8.7	8.5 ± 0.5
10	*S. hyperborea str. 2*	μ	4.4 ± 0.0	> 8.7	> 8.7	> 8.7	> 8.7
10	*S. hyperborea str. 2*	k	3.5 ± 0.6	4.4 ± 0.9	0.9 ± 0.5	5.3 ± 0.6	7.1 ± 0.4
50	*F. cylindrus*	μ	> 8.7	8.0 ± 0.1	> 8.7	8.4 ± 0.0	7.9 ± 0.0
50	*F. cylindru*	k	8.4 ± 0.3	7.1 ± 0.1	> 8.7	8.1 ± 0.1	7.6 ± 0.1

Modeling the Impact of a Crude Oil Spill on a Sea Ice Algal Spring Bloom

To better understand how an ANS crude oil spill might impact the diversity and biomass of sea ice algae in the Arctic, a 1D model was used to simulate an oil spill before the spring bloom. Two conditions were evaluated, without oil (0.0 mg l^{-1} of TPH), and at the highest tested concentration (8.7 mg l^{-1} of TPH). The seasonal irradiance and sea ice thickness were forced by data from the National Ecological Observatory Network at the Utqiaġvik, Alaska station and the sea ice mass balance station in the Chukchi Sea respectively. The ice thickness data used in this model reached a maximum thickness of 1.37 m before decreasing and calculated under-ice irradiances reached maximum values of approximately 40, 13, and 4.5 μmols photons m^{-2} s^{-1} under snow depths of 0, 0.1, and 0.2 m respectively. Results from the 1D model show that a lower irradiance due to attenuation by snow depth, and oil exposure, alters community composition and diatom biomass (Figure 8). *F. cylindrus* performs best under conditions of low

snow (< 0.05 m) without crude oil contamination (Figure 8A) and makes up a negligible proportion of the community when crude oil is present (Figure 8B). *A. spetentrionalis* was most abundant under moderate snow conditions (0.10 m) without crude oil contamination (Figure 8A) and highest snow conditions (0.2 m) in the presence of oil contamination (Figure 8B). *S. hyperborea* strains were most abundant at high snow conditions (0.2 m) in the absence of crude oil contamination (Figure 6A) and dominated the diatom community in the presence of crude oil contamination (Figure 8B) under all snow conditions. Predicted biomass declined with increasing snow depth (Figure 8C, E). Crude oil-exposed communities generated less biomass than the unexposed spring bloom communities (< 51%), but particularly without snow (< 3%; Figure 8C).

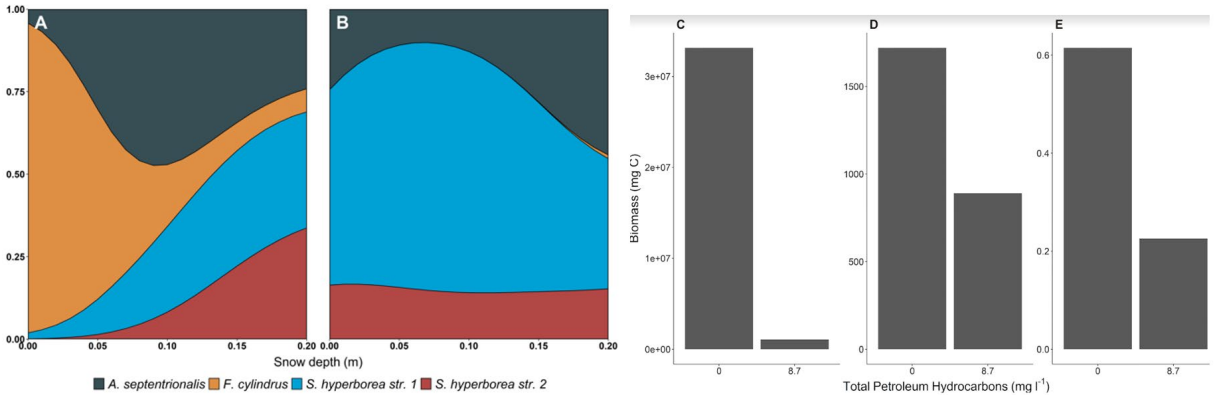

Figure 8. Modeled sea ice diatom composition and biomass modified by snow depth and crude oil spill. Sea ice diatom community composition in unoiled (A) and exposure to ANS crude oil spill (B) scenarios over a range of snow depths (m) at the end of a modeled spring bloom. Modeled sea ice diatom biomass (mg C) in low snow: 0 m (C), moderate snow 0.1 m (D), and high snow 0.2 m (E) with and without a simulated ANS crude oil spill.

Table 4. Summary of crude oil analyses for transcriptome experiments. Water accommodated fractions (WAF %) of ANS crude oil contaminated water and their concentrations (mg L^{-1}) for Total Petroleum Hydrocarbons (TPH), Diesel Range Organics (DRO), Residual Range Organics (RRO) and Gas Range Organics (GRO) for each species or natural community subject to transcriptome experiments.

Species	WAF (%)	TPH	DRO	RRO	GRO
F. cylindrus	92	6.2	2.2	0.3	-
F. cylindrus	47	3.6	1.1	0.2	-
S. hyperborea	92	7.9	2.4	0.2	-
S. hyperborea	47	3.9	1.2	0.1	-
Natural Community	47	6.2	2.2	0.3	8.9

Gene Expression and Community Composition Changes with Crude Oil Contamination

To assess the gene expression response of diatoms to crude oil contamination and test the predictions of our 1D model, we performed batch experiments on sea ice diatom isolates (*F. cylindrus* and *S. hyperborea*) and natural sea ice communities from Utqiaġvik, Alaska. The

diatom isolates were grown in larger volumes (~2 L) to generate enough biomass for RNA extraction and sequencing. ANS crude oil WAF was generated as described previously to test the impact of 92 and/or 47% WAF (Table 4) under three light levels (ranging from 3–125 µmols photons m^{-2} s^{-1}). The crude oil analysis revealed that the TPH concentrations varied by WAF batch (Table 4), but were similar to those used in the plate experiments to determine dose-response curves for these sea ice diatoms.

Batch experiments revealed markedly higher impacts of ANS crude oil on growth rates for *Fragilariopsis cylindrus* and *Synedropsis hyperborea* isolates (Figure 9) compared to the impacts measured for the same species in the plate experiments (Figures 6 and 7). Chlorophyll *a* fluorescence of batch cultured isolates was significantly lower in both 42% and 82% WAF treatments compared to control (0% WAF) after 2–5 days in all light levels. *S. hyperborea* appeared to be less sensitive than *F. cylindrus* at 42% WAF, displaying positive growth in 42% WAF at 20 and 125 µmols photons m^{-2} s^{-1}, whereas *F. cylindrus* had flat or declining chlorophyll *a* concentration in most crude oil treatments and irradiances. Filters from each experiment were collected and RNA was extracted from the control and 42% WAF experiments. RNA was extracted and sequenced, but the analysis is ongoing for this part of the project.

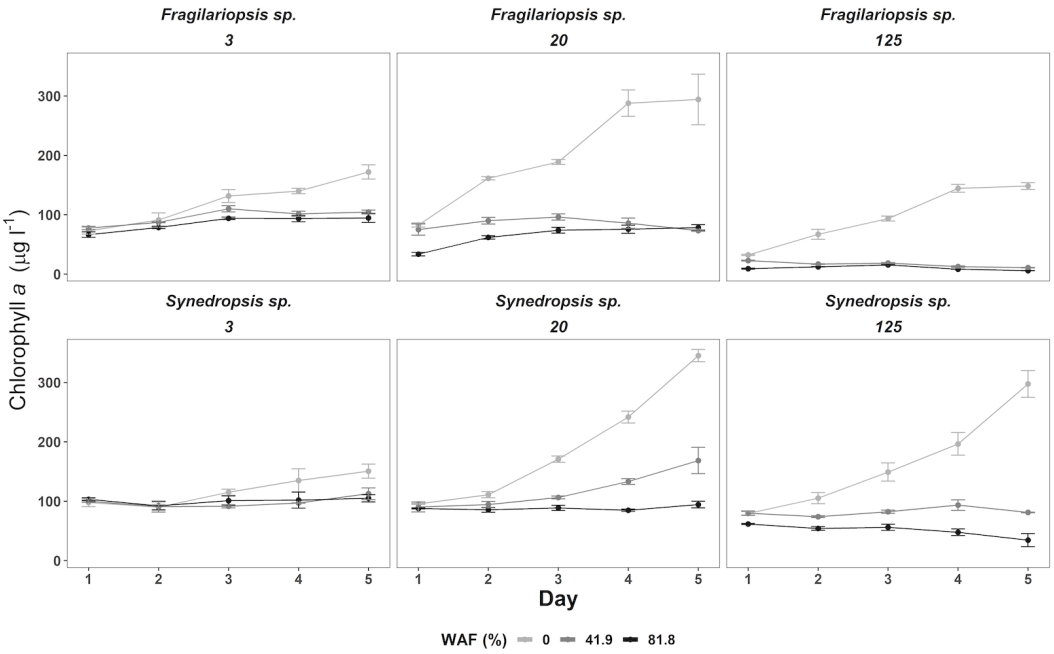

Figure 9. Chlorophyll *a* fluorescence growth curves for sea ice diatoms grown in batch culture. Colors of the lines and points represent WAF (%) treatment as in the legend for three light levels (3, 20, and 125 µmols photons m^{-2} s^{-1}) for two isolates (*Fragilariopsis cylindrus* and *Synedropsis hyperborea*). Error bars represent the standard deviation based on triplicate bottles.

Similarly, natural sea ice communities were strongly impacted by crude oil contamination at all light levels (Figure 10). With a significant separation in chlorophyll *a* concentration at low light (15 µmols photons m^{-2} s^{-1}) by day 5 and a significant separation at moderate (40 µmols

photons m^{-2} s^{-1}) and high (125 µmols photons m^{-2} s^{-1}) by day 10. In the natural community batch culture experiment, all treatments had an initial decrease in chlorophyll *a* concentration, which can be attributed to a lag phase or initial die-off under laboratory conditions. Filters were collected from each experiment, but they have yet to be extracted and sequenced.

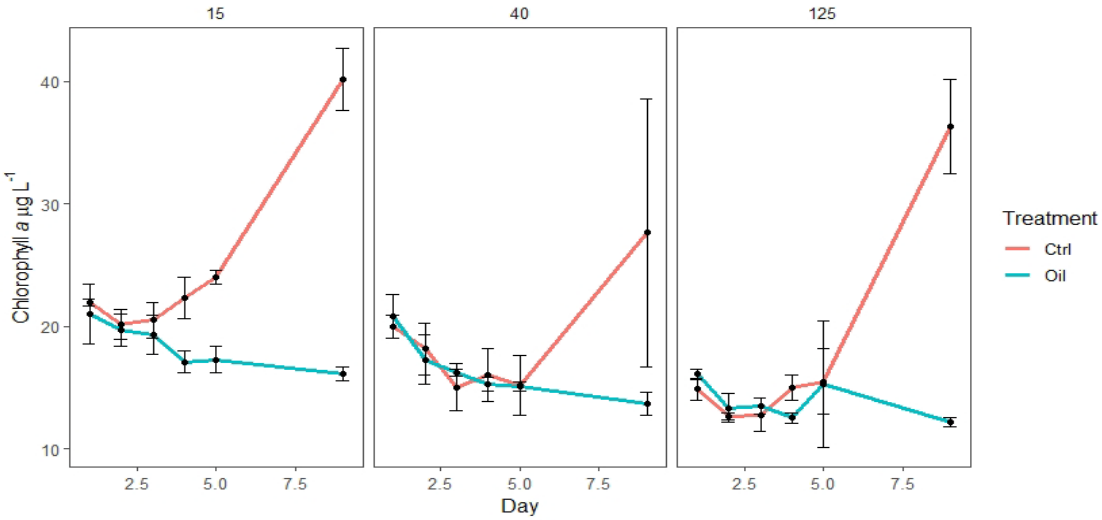

Figure 10. Chlorophyll *a* fluorescence growth curves for natural sea ice communities grown in batch culture. Mean chlorophyll *a* measured daily at each of the three irradiances during the experiment (15, 40, and 125 µmols photons m^{-2} s^{-1}). Colors represent ANS WAF treatments: control (0% WAF) and oil (42% WAF), and error bars represent the standard deviation based on triplicate bottles.

DISCUSSION

Taxon-specific ANS Crude Oil Sensitivity

In this study, we used high-throughput plate cultures to determine the sublethal inhibition of sea ice diatoms by ANS crude oil WAF. This allowed us to create high-resolution (12-point) dose-response curves for five irradiances, whereas most studies only test a few WAF treatments. The sea ice diatoms in this study had a range of sensitivities to ANS crude oil-contaminated media. The most sensitive was *F. cylindrus* with IC_{10} of 1.4–5.3 mg L^{-1} and IC_{50} of 7.9–8.4 mg L^{-1} for growth (Table 3) with a clear decrease in growth rates around 6.0 mg L^{-1} across irradiances. This contrasted with other sea ice diatoms isolated from the same sea ice that had IC_{10} measurable only for some irradiances and which did not have measurable IC_{50} over the range of concentrations tested (Table 3). These results are similar to previous studies showing a range of sensitivities by phytoplankton taxa and hydrocarbon composition (Echeveste et al. 2010, 2016). Stimulation of growth by low levels of hydrocarbons has also been noted in studies of phytoplankton toxicology as we saw for a few of the irradiance treatments of *S. hyperborea* and *A. septentrionalis* (Figure 6), such a response could be indicative of cell metabolism ramping up in response to the toxin.

Why do we observe such large differences in ANS crude oil sensitivity between these diatoms? Echeveste et al. (2016) suggested that cell biovolume was one of the most important factors

influencing differences in phytoplankton sensitivity to organic pollutants. We did not find a significant relationship between biovolume and ANS crude oil sensitivity in this study however there was a limited range of biovolumes between these four taxa (Table 1), with a larger number of sea ice algae we may have been able to detect this effect. Another notable difference between sea ice diatom strains is in the maximum growth rates and photophysiology (Figure 5, Table 2); *F. cylindrus* has the highest maximum growth rate and is best adapted to high light conditions. Higher basal metabolic rates may make *F. cylindrus* more sensitive to the additional ROS generated by organic pollutants as higher metabolic rates are associated with greater ROS production. Additionally, we note that both *S. hyperborea* strains formed biofilms in the plate experiments, whereas the other strains were largely suspended in the contaminated media. Biofilm formation can restrict the flow of nutrients or pollutants to algal cells by reducing the surface area that is exposed to the media. Further evidence that the lack of sensitivity may be due to biofilm formation is that the maximum cell densities of S. hyperborea were impacted by ANS crude oil contamination (Figure 7) to a greater extent than growth rates were inhibited (Figure 6). This suggests that biofilm formation protected *S. hyperborea* from growth inhibition until the culture reached a critical cell density and ran out of surfaces to colonize. We postulate that this effect could be protective in the event of a crude oil spill in the early spring, but less helpful in late bloom. We also note that these cultures while uni-algal are non-axenic and therefore we cannot eliminate the possibility that differences in associated bacteria may be important in modifying crude oil sensitivity.

Interactions Between Crude Oil Sensitivity and Irradiance

As we expected, we observed interactions between crude oil and irradiance treatments in terms of growth physiology. For example, *A. septentrionalis* had a significantly lower IC_{10} and was therefore more sensitive at high light compared with low to moderate light conditions (Table 3, Figure 6). Exacerbation of crude oil sensitivity by high light was as we hypothesized due to the additive impacts of ROS. Surprisingly, other taxa investigated in our study showed the opposite or mixed interaction between crude oil sensitivity and irradiance. *S. hyperborea* strains appeared to be more sensitive to ANS crude oil contamination at the lowest light level tested (Table 3, Figures 6 and 7). Similarly, *F. cylindrus* was more sensitive at low to moderate light levels (10-20 µmols photons m^{-2} s^{-1}). These results suggest that these diatoms may employ an energy-dependent strategy for detoxifying organic pollutants found in ANS crude oil or that being pre-acclimated to higher light could increase the expression of ROS detoxification mechanisms thus allowing these cells to be pre-conditions to deal with additional ROS generation by organic pollutants. The analysis of transcriptome and metatranscriptome data of sea ice algae subject to crude oil contamination over a range of irradiances should help to clarify the intracellular response mechanisms.

Spring Bloom Model Interpretation

Using our empirical dose-response curves for these four sea ice diatoms plus *in situ* estimates of under-ice irradiance, we created a 1D model to estimate biomass and community

composition in the event of an oil spill under a range of snow cover scenarios. The simulated sea ice diatom community was most diverse at moderate snow levels in the absence of a crude oil spill, (Figure 8A). At low snowpack, the evenness was lower, with the *F. cylindrus* dominating the community and producing the highest biomass (Figure 8A). In the case of a simulated crude oil spill (Figure 8B), species diversity and evenness both decline at all light levels largely due to the detrimental impacts on *F. cylindrus* (Figure 8B). Biomass also declines sharply in all snow conditions (Figures 8C, D), particularly with no snow or bare ice (Figure 8C). These results suggest that impacts in the early spring would be worse in a low snow year due to the higher sensitivity of diatoms like *F. cylindrus*, which are better adapted to higher light conditions.

Here, we need to introduce a few important caveats for model interpretation. First, this is a very simple model, only seeded with the four strains of sea ice diatoms investigated in this study, so it is missing much of the natural diversity in the system. However, the model predictions of diversity are what we might suppose, with intermediate conditions (without a crude oil spill) creating the best circumstances for species co-existence. Second, we caution that biomass estimates for this model are particularly uncertain as we chose to parameterize grazing as a constant exponential loss term, whereas most modeled grazing rates would be density dependent. A density-dependent grazing rate could substantially reduce the biomass in the highest density cases, but grazing is also likely to be altered as zooplankton metabolism is impacted by crude oil toxicity (Lemcke et al. 2019). To avoid parameterizing grazing without sufficient data, we chose a simple constant rate. Third, the model assumes incoming irradiance as a sole limiting factor (no nutrient limitation, no self-shading), which should be a good assumption for early in the spring bloom, but invalid for the later stages of a spring bloom. Light limitation may also be an issue with a dense oil slick adhering to the sea ice. For this model, we only considered crude oil water accommodated fraction (WAF), which is so dilute that light attenuation is negligible. Finally, this 1D model does not allow for considering the lateral dispersal of oil or microbial communities, but it could be expanded to make it spatially explicit in the future.

Given these caveats and the simplistic assumptions of the 1D model, we suggest the model results should be used as only a preliminary tool to understand the first-order impacts of a crude oil spill under various snow scenarios. Though additional factors and parameters need to be incorporated into a model to produce accurate predictions of sea ice algal diversity or biomass, we posit that this model is a useful way to contextualize the data from our study.

Batch/Transcriptome Experiments and Future Analysis

Following up on the results of the high-throughput plate experiments and model predictions, we sought to understand the intracellular response of sea ice diatoms by using gene expression and amplicon sequencing analyses. We scaled up the experiments to 2L batch cultures to get adequate biomass for RNA and DNA extractions. The experiments were performed first with sea ice diatom isolates with contrasting responses to crude oil contamination: *F. cylindrus* and *S. hyperborea*. In the plate experiments, *S. hyperborea* had little to no change in growth rate over a range of ANS crude oil concentrations and irradiances. However, in batch cultures, we saw a marked decrease in chlorophyll *a* concentration in moderate to high WAF treatments. The

difference observed between plate and batch culture experiments could be explained by the need to gently invert the bottles in batch culture experiments for each daily sampling point, thereby mixing up the algal cells and preventing them from forming biofilms that may have a protective role as noted above. We hypothesize these methodological differences increased the effective exposure level for *S. hyperborea* in particular as *F. cylindrus* did not form visible biofilms in the plate experiments. We posit that batch experiments are more representative of the conditions these algae would be exposed to in the planktonic phase and the plate experiments are a better analog for sea ice habitats. These results suggest that phytoplankton may be more at risk for ANS crude oil toxicity than sea ice algae due to greater surface area for exposure.

Natural sea ice communities were similarly sensitive to crude oil contamination in batch experiments, but this may be an overestimate of their sensitivity if sea ice habitats allow these species to form protective biofilms. We also note that natural sea ice communities had an initial decline in both control and WAF treatments for the first few days under all irradiances. This initial lag/die-off phase is common for environmental microbes acclimating to new conditions in the laboratory and likely reflects the stress of bottle effects and transport. DNA extractions are complete for these experiments, but we do not yet have the sequences to see if the model predictions will be borne out by the results. We expect a decrease in algal diversity with oil contamination, particularly under the highest light conditions. Preliminary microscopy of the samples found high concentrations of *Fragilariopsis spp*., so we expect that these species will be particularly sensitive to crude oil contamination as in our isolate experiments. This analysis is still ongoing and we do not yet have results to report on the gene expression changes in sea ice diatoms and natural communities exposed to ANS crude oil under varying irradiances, however, we anticipate that these data will help us interpret the differences in physiology observed in both plate and batch experiments.

CONCLUSIONS

We showed that ANS crude oil-contaminated seawater differentially impacted the growth of sea ice diatoms (isolated from near Utqiaġvik, Alaska) based on species and irradiance. Our results suggest that diatoms adapted to higher light, such as *Fragilariopsis cylindrus*, may be more sensitive to ANS oil-contaminated seawater. Therefore, in conditions with low snow cover and/or thinner sea ice in the Alaskan Arctic, an oil spill would be predicted to have a larger adverse impact on diatom growth and diversity. We further tested these predictions with natural communities of sea ice algae under *in situ* light conditions. Gene expression analysis from this study is ongoing, but we hope to determine genetic markers of diatom responses to crude oil contamination that could be used as indicators of the ecosystem impact of a potential spill. More work remains to be done to determine the ecological implications and drivers of shifts in sea ice diatom diversity (e.g., Does the nutritional quality of sea ice diatoms differ? Does sea ice bacteria participate in ameliorating/exacerbating crude oil toxicity?). Despite its limitations, this study provides important data to understand the potential impact of ANS crude oil toxicity on sea ice algae. This work has important implications for our ability to assess the potential for ecosystem disruption in the event of a crude oil spill in the Alaskan Arctic.

ACKNOWLEDGMENTS

We are grateful for funding from BOEM/CMI (M20AC10007) and matching funds provided from the State of Alaska. We received additional student support from the College of Fisheries and Ocean Sciences, fieldwork support from Ukpeaġvik Iñupiat Corporation (UIC) and Marc Oggier, and facilities/resources from the UAF Imaging Center and UAF Genomics Core Lab.

STUDY PRODUCTS

Educational Materials

The Hidden World within Sea Ice. Educational kit available for loan, UAF Museum of the North, Fairbanks, AK. https://www.uaf.edu/museum/education/educators/kits-hands-on-objects

Presentations

Dilliplaine, K., and G. M. M. Hennon. (2021). Impact of sublethal oil exposure and irradiance on sea ice algae. Oral presentation (virtual), Alaska Marine Science Symposium, Anchorage, AK.

Hennon, G. M. M. (2021). Towards predicting climate change impacts on phytoplankton communities from the Subtropics to the Arctic. Oral presentation (virtual), NOAA Northwest Fisheries Science Center Seminar, Juneau, AK.

Dilliplaine, K., and G. M. M. Hennon. (2021). Diatoms on thin ice: sensitivity and resiliency to anthropogenic change in the Alaskan Arctic. Invited speaker, Molecular Life of Diatoms 6, Virtual Workshop, Scripps Institution of Oceanography, San Diego, CA.

Dilliplaine, K. (2021) Investigating the impacts of oil exposure and changing snow cover on sea ice microbial communities. College of Fisheries and Ocean Sciences Seminar, University of Alaska Fairbanks, Fairbanks, AK.

Dilliplaine, K. D., and G. M. M. Hennon. (2022). Sea ice diatom sensitivity to sublethal crude oil exposure in a brighter Arctic. Oral presentation (virtual), Alaska Marine Science Symposium, Anchorage, AK.

Dilliplaine, K., and G. M. M. Hennon. (2022). Sea ice algal response to sublethal oil exposure at varying irradiance levels. Poster presentation, Biogeochemical Exchange Processes at the Sea Ice Interface (BEPSII) field school, Cambridge Bay, CAN.

Publications

Dilliplaine, K., and G. M. M. Hennon. Irradiance modifies impact of crude oil exposure on sea ice diatoms in the Alaskan Arctic. (in prep) Elementa Science of the Anthropocene.

Dilliplaine, K., and G. M. M. Hennon. Gene expression signatures of sea ice diatoms exposed to crude oil. (in prep) Ecotoxicology or similar journal.

REFERENCES

Alaska Department of Environmental Conservation (ADEC). 2002a. Method AK 102 For Determination of Diesel Range Organics (Version 04/08/02). Anchorage, AK. Available at http//dec.alaska.gov/media/13473/ak-10-2.pdf

Alaska Department of Environmental Conservation (ADEC). 2002b. Method AK 103 For Determination of Residual Range Organics (Version 04/08/02). Anchorage, AK. Available at http//dec.alaska.gov/media/13474/ad-10-03.pdf

Aksmann, A., and Z. Tukaj. 2008. Intact anthracene inhibits photosynthesis in algal cells: A fluorescence induction study on *Chlamydomonas reinhardtii* cw92 strain. Chemosphere **74**: 26–32. doi:10.1016/j.chemosphere.2008.09.064

Arctic Monitoring and Assessment Programme (AMAP). 2007. Assessment 2007: Oil and Gas Activities in the Arctic - Effects and Potential Effects, Volumes 1 and 2. Oslo, NOR.

Arctic Council. 2009. Arctic Marine Shipping Assessment 2009 Report. Tromso, NOR. Available at https://oaarchive.arctic-council.org/handle/11374/54

Aurand, D., and G. M. Coelho. 2005. Cooperative Aquatic Toxicity Testing of Dispersed Oil and the Chemical Response to Oil Spills: Ecological Effects Research Forum (CROSERF). Technical Report 07-03. Lusby, MD

Beckman, K. B., and B. N. Ames. 1997. Oxidative decay of DNA. Journal of Biological Chemistry **272**: 19633–19636. doi:10.1074/jbc.272.32.19633

Berlett, B. S., and E. R. Stadtman. 1997. Protein oxidation in aging, disease, and oxidative stress. Journal of Biological Chemistry **272**: 20313–20316. doi:10.1074/jbc.272.33.20313

Blanken, H., L. B. Tremblay, S. Gaskin, and A. Slavin. 2017. Modelling the long-term evolution of worst-case Arctic oil spills. Marine Pollution Bulletin **116**: 315–331. doi:10.1016/j.marpolbul.2016.12.070

Boccadoro, C., A. Krolicka, J. Receveur, C. Aeppli, and S. Le Floch. 2018. Microbial community response and migration of petroleum compounds during a sea-ice oil spill experiment in Svalbard. Marine Environmental Research **142**: 214–233. doi:10.1016/j.marenvres.2018.09.007

Boetius, A., S. Albrecht, K. Bakker, and others. 2013. Export of algal biomass from the melting Arctic sea ice. Science **339**:1430–1432. doi:10.1126/science.1231346

Bowman, J. S. 2015. The relationship between sea ice bacterial community structure and biogeochemistry: A synthesis of current knowledge and known unknowns. Elementa: Science of the Anthropocene **3**: 000072. doi:10.12952/journal.elementa.000072

Burnham, K. P., and D. R. Anderson. 2004. Multimodel inference. Sociological Methods Research **33**: 261–304. doi:10.1177/0049124104268644

Dilliplaine, K., M. Oggier, R. Gradinger, H. Eicken, E. Collins, and B. Bluhm. 2021. Crude oil exposure prevents ice algal bloom in a sea-ice mesocosm experiment. Polar Biology **44:** 525–537. doi:10.1007/s00300-021-02818-3

Echeveste, P., S. Agustí, and J. Dachs. 2010. Cell size-dependent toxicity thresholds of polycyclic aromatic hydrocarbons to natural and cultured phytoplankton populations. Environmental Pollution **158**: 299–307. doi:10.1016/j.envpol.2009.07.006

Echeveste, P., C. Galbán-Malagón, J. Dachs, N. Berrojalbiz, and S. Agustí. 2016. Toxicity of natural mixtures of organic pollutants in temperate and polar marine phytoplankton. Science of the Total Environment **571**: 34–41. doi:10.1016/j.scitotenv.2016.07.111

Eguíluz, V. M., J. Fernández-Gracia, X. Irigoien, and C. M. Duarte. 2016. A quantitative assessment of Arctic shipping in 2010-2014. Scientific Reports **6**: 3–8. doi:10.1038/srep30682

Eilers, P. H. C., and J. C. H. Peeters. 1988. A model for the relationship between light intensity and the rate of photosynthesis in phytoplankton. Ecological Modelling **42**: 199–215. doi:10.1016/0304-3800(88)90057-9

El-Sheekh, M. M., R. A. Hamouda, and A. A. Nizam. 2013. Biodegradation of crude oil by *Scenedesmus obliquus* and *Chlorella vulgaris* growing under heterotrophic conditions. International Biodeterioration and Biodegradation **82**: 67–72. doi:10.1016/j.ibiod.2012.12.015

Gardiner, W. W., J. Q. Word, J. D. Word, R. A Perkins, K. M. McFarlin, B. W. Hester, L. S. Word, and C. M. Ray. 2013. The acute toxicity of chemically and physically dispersed crude oil to key Arctic species under Arctic conditions during the open water season. Environmental Toxicology and Chemistry **32**: 2284–2300. doi:10.1002/etc.2307

Garneau, M.-È., C. Michel, G. Meisterhans, N. Fortin, T. L. King, C. W. Greer, and K. Lee. 2016. Hydrocarbon biodegradation by Arctic sea-ice and sub-ice microbial communities during microcosm experiments, Northwest Passage (Nunavut, Canada). FEMS Microbial Ecology **92**: fiw130. doi:10.1093/femsec/fiw130

Garrison, D. L., and K. R. Buck. 1986. Organism losses during ice melting: A serious bias in sea ice community studies. Polar Biology **6**: 237–239. doi:10.1007/BF00443401

Ghosal, D., S. Ghosh, T. K. Dutta, and Y. Ahn. 2016. Current state of knowledge in microbial degradation of polycyclic aromatic hydrocarbons (PAHs): A review. Frontiers in Microbiology **7**. doi:10.3389/fmicb.2016.01369

Gilde, K., and J. L. Pinckney. 2012. Sublethal effects of crude oil on the community structure of estuarine phytoplankton. Estuaries and Coasts **35**: 853–861. doi:10.1007/s12237-9473-8

Guillard, R. R., and J. H. Ryther. 1962. Studies of marine planktonic diatoms. I. Cyclotella nana Hustedt, and *Detonula confervacea (cleve) Gran*. Canadian Journal of Microbiology **8**: 229–239. doi:10.1139/m62-029

Gutteridge, J. M. C. 1995. Lipid peroxidation and antioxidants as biomarkers of tissue damage. Clinical Chemistry **41**: 1819–1828.

Hall, B. G., H. Acar, A. Nandipati, and M. Barlow. 2014. Growth rates made easy. Molecular Biology and Evolution **31**: 232–238. doi:10.1093/molbev/mst187

Hasle, G. R., L. K. Medlin, and E. E. Syvertsen. 1994. *Synedropsis gen. nov*., a genus of araphid diatoms associated with sea ice. Phycologia **33**: 248–270. doi:10.2216/i0031-8884-33-4-248.1

Hennon, G. M. M., J. Ashworth, R. D. Groussman, C. Berthiaume, R. L. Morales, N. S. Baliga, M. V. Orellana, and E. V. Armbrust. 2015. Diatom acclimation to elevated CO_2 via cAMP signaling and coordinated gene expression. Nature Climate Change **5**: 761–766. doi:10.1038/nclimate2683

Hennon, G. M. M., J. J. Morris, S. T. Haley, E. R. Zinser, A. Durrant, E. Entwistle, T. Dokland, and S. T. Dyhrman. 2018. The impact of elevated CO_2 on *Prochlorococcus* and microbial interactions with 'helper' bacterium *Alteromonas*. ISME **12**: 520–531. doi:10.1038/ismej.2017.189

Hong, Y. W., D. X. Yuan, Q. M. Lin, and T. L. Yang. 2008. Accumulation and biodegradation of phenanthrene and fluoranthene by the algae enriched from a mangrove aquatic ecosystem. Marine Pollution Bulletin **56**: 1400–1405. doi:10.1016/j.marpolbul.2008.05.003

Hsiao, S. I. C. 1978. Effects of crude oils on the growth of arctic marine phytoplankton. Environmental Pollution **17**: 93–107. doi:10.1016/0013-9327(78)90043-5

Jassby, A. D., and T. Platt. 1976. Mathematical formulation of the relationship between photosynthesis and light for phytoplankton. Limnology and Oceanography **21**: 540–547. doi:10.4319/lo.1976.21.4.0540

Juhl, A. R., and C. Krembs. 2010. Effects of snow removal and algal photoacclimation on growth and export of ice algae. Polar Biology **33**: 1057–1065. doi:10.1007/s00300-010-0784-1

Kimura, K., and Y. Tomaru. 2013. A unique method for culturing diatoms on agar plates. Plankton and Benthos Research **8**: 46–48. doi:10.3800/pbr.8.46

Knezevic, S. Z., J. C. Streibig, and C. Ritz. 2007. Utilizing R software package for dose-response studies: The concept and data analysis. Weed Technology **21**: 840–848. doi:10.1614/WT-06-161.1

Kohlbach, D., S. H. Ferguson, T. A. Brown, and C. Michel. 2019. Landfast sea ice-benthic coupling during spring and potential impacts of system changes on food web dynamics in Eclipse Sound, Canadian Arctic. Marine Ecology Progress Series **627**: 33–48.

Kohlbach, D., M. Graeve, B. A. Lange, C. David, I. Peeken, and H. Flores. 2016. The importance of ice algae-produced carbon in the central Arctic Ocean ecosystem: Food web relationships revealed by lipid and stable isotope analyses. Limnology and Oceanography **61**: 2027–2044. doi:10.1002/lno.10351

Lee, S. H., T. E. Whitledge, and S. H. Kang. 2008. Springtime production of bottom ice algae in the landfast sea ice zone at Barrow, Alaska. Journal of Experimental Marine Biology and Ecology **367**: 204–212. doi:10.1016/j.jembe.2008.09.018

Lemcke, S., J. Holding, E. F. Møller, J. Thyrring, K. Gustavson, T. Juul-Pedersen, and M. K. Sejr. 2019. Acute oil exposure reduces physiological process rates in Arctic phyto- and zooplankton. Ecotoxicology **28**: 26–36. doi:10.1007/s10646-018-1995-4

Lomas, M. W., S. E. Baer, S. Acton, and J. W. Krause. 2019. Pumped Up by the Cold: Elemental Quotas and Stoichiometry of Cold-Water Diatoms. Frontiers in Marine Science **6**. doi:10.3389/fmars.2019.00286

Manes, S. S., and R. Gradinger. 2009. Small scale vertical gradients of Arctic ice algal photophysiological properties. Photosynthesis Research 53–66. doi:10.1007/s11120-009-9489-0

Mcdonald, S., T. Koulis, J. Ehn, K. Campbell, M. Gosselin, and C. J. Mundy. 2015. A functional regression model for predicting optical depth and estimating attenuation coefficients in sea-ice covers near Resolute Passage, Canada. Annals of Glaciology **56**: 147–154. doi:10.3189/2015AoG69A004

Mcfarlin, K. M., R. A. Perkins, W. W. Gardiner, J. D. Word, and J. Q. Word. 2011. Toxicity of Physically and Chemically Dispersed Oil to Selected Arctic Species. 2011 International Oil Spill Conference Proceedings. International Oil Spill Conference. doi:10.7901/2169-3358-2011-1-149

Michel, C., R. G. Ingram, and L. R. Harris. 2006. Variability in oceanographic and ecological processes in the Canadian Arctic Archipelago. Progress in Oceanography **71**: 379–401. doi:10.1016/j.pocean.2006.09.006

National Science Foundation Arctic Data Center. 2009. Automated ice mass balance site (SIZONET).doi:10.18739/A2BM0G

Overland, J. E., and M. Wang. 2013. When will the summer Arctic be nearly sea ice-free? Geophysical Research Letters **40**: 2097–2101. doi:10.1002/grl.50316

Ozhan, K., S. M. Miles, H. Gao, and S. Bargu. 2014. Relative phytoplankton growth responses to physically and chemically dispersed South Louisiana sweet crude oil. Environmental Monitoring and Assessment **186**: 3941–3956. doi:10.1007/s10661-014-3670-4

Ozhan, K., S. Zahraeifard, A. P. Smith, and S. Bargu. 2015. Induction of reactive oxygen species in marine phytoplankton under crude oil exposure. Environmental Science and Pollution Research **22**: 18874–18884. doi:10.1007/s11356-015-5037-y

Parker, M. S., and E. V. Armbrust. 2005. Synergistic effects of light, temperature, and nitrogen source on transcription of genes for carbon and nitrogen metabolism in the centric diatom *Thalassiosira pseudonana* (Bacillariophyceae). Journal of Phycology **41**: 1142–1153. doi:10.1111/j.1529-8817.2005.00139.x

Platt, T., C. L. Gallegos, and W. G. Harrison. 1980. Photoinhibition and photosynthesis in natural assemblages of marine phytoplankton. Journal of Marine Research **38**: 687–701.

Polyakov, I. V, A. V Pnyushkov, M. B. Alkire, and others. 2017. Greater role for Atlantic inflows on sea-ice loss in the Eurasian Basin of the Arctic Ocean. Science (1979) **356**: 285 LP – 291. doi:10.1126/science. aai8204

Poulin, M., N. Daugbjerg, R. Gradinger, L. Ilyash, T. Ratkova, and C. von Quillfeldt. 2011. The pan-Arctic biodiversity of marine pelagic and sea-ice unicellular eukaryotes: A first-attempt assessment. Marine Biodiversity **41**: 13–28. doi:10.1007/s12526-010-0058-8

Ropeik, A. 2015. Arctic Barge Nears Russia After Months in Ice. Alaska Public Media. https://alaskapublic.org/2015/02/26/arctic-barge-nears-russia-after-months-in-ice/

Schneider, C. A., W. S. Rasband, and K. W. Eliceiri. 2012. NIH Image to ImageJ: 25 years of image analysis. Nature Methods **9**: 671–675. doi:10.1038/nmeth.2089

Sikkema, J., J. A. M. De Bont, and B. Poolman. 1995. Mechanisms of membrane toxicity of hydrocarbons. Microbiological Reviews **59**: 201–222.

Silsbe, G., and S. Malkin. 2015. Phytotools: phytoplankton production tools. R package version 1.0. Available at https://rdrr.io/cran/phytotools

Singer, M. M., D. Aurand, G. E. Bragin, J. R. Clark, G. M. Coelho, M. L. Sowby, and R. S. Tjeerdema. 2000. Standardization of the preparation and quantitation of water-accommodated fractions of petroleum for toxicity testing. Marine Pollution Bulletin **40**: 1007–1016. doi:10.1016/S0025-326X (00)00045-X

Spiess, A.-N., and N. Neumeyer. 2010. An evaluation of R2 as an inadequate measure for nonlinear models in pharmacological and biochemical research: a Monte Carlo approach. BMC Pharmacology **10**: 6. doi:10.1186/1471-2210-10-6

Szymanski, A., and R. Gradinger. 2016. The diversity, abundance, and fate of ice algae and phytoplankton in the Bering Sea. Polar Biology **39**: 309–325. doi:10.1007/s00300-015-1783-z

Wang, M., Q. Yang, J. E. Overland, and P. Stabeno. 2018. Sea-ice cover timing in the Pacific Arctic: The present and projections to mid-century by selected CMIP5 models. Deep-Sea Research Part II: Topical Studies in Oceanography **152**: 22–34. doi:10.1016/j.dsr2.2017.11.017

Webb, W. L., M. Newton, and D. Starr. 1974. Carbon dioxide exchange of *Alnus rubra*. Oecologia **17**: 281–291. doi:10.1007/BF00345747

The Department of the Interior Mission

As the Nation’s principal conservation agency, the Department of the Interior has responsibility for most of our nationally owned public lands and natural resources. This includes fostering the sound use of our land and water resources, protecting our fish, wildlife and biological diversity; preserving the environmental and cultural values of our national parks and historical places; and providing for the enjoyment of life through outdoor recreation.The Department assesses our energy and mineral resources andworks to ensure that their development is in the best interests of all our people by encouraging stewardship and citizen participation in their care. The Department also has a major responsibility for American Indian reservation communities and for people who live in island communities.

The Bureau of Ocean Energy Management

The Bureau of Ocean Energy Management (BOEM) works to manage the exploration and development of the nation's offshore resources in a way that appropriately balances economic development, energy independence, and environmental protection through oil and gas leases, renewable energy development and environmental reviews and studies.